Journal of Solid State Chemistry **157,** 193–205 (2001)
doi:10.1006/jssc.2000.9075, available online at http://www.idealibrary.com on IDEAL®

Electronic Band Structure of TlTe

Frank R. Wagner*,[1] and Klaus Stöwe†

*Max-Planck-Institut für Chemische Physik fester Stoffe, Nöthnitzer Straße 40, 01187 Dresden, Germany; and
†Institut für Anorganische Chemie und Analytische Chemie und Radiochemie, Universität des Saarlandes, 66041 Saarbrücken, Germany

Received August 29, 2000; in revised form November 21, 2000; accepted December 8, 2000

We report about self-consistent ab initio LMTO-ASA calculations of the electronic band structure and the crystal orbital Hamiltonian population function COHP. The calculations support a view of TlTe as an univalent Tl compound with two polyanionic partial structures, linear branched and unbranched chains, characterized by 3c–4e type of bonding, both within the chains and within the branches. The system deviates from classical Peierls-type systems with respect to the lack of energetic separation of the two types of transition-driving σ bands due to the appearance of nonintrachain bands close to E_F. Tl coordination causes the lack of elastic degrees of freedom, which prevents the system from introducing completely alternating chains in one step. The branched Te2 chains are shown to be favored for pairing distortion compared to Te3 chains as a result of the weaker Tl–Te2 interactions. The distortion is interpreted as a dimerization of $(Te_3)^{3-}$ units to form a new type of 42 electron $(Te_6)^{6-}$ partial structure not known in polyhalogenide or noble gas halogenide chemistry. © 2001 Academic Press

INTRODUCTION

The correct room temperature (RT) structure of TlTe has been known since the work of Weis *et al.* in 1974 (1). Recently (2), the structure of a low-temperature (LT) phase occurring at $T = 172$ K was solved and the crystal chemical aspects of the structural phase transition were discussed.

The room temperature phase (space group $I4/mcm$) consists of three crystallographically and chemically different Te atoms, Te1, Te2, and Te3, which form two different types of linear equidistant chains along [001]: One type of chain consists solely of Te3 atoms at distances d(Te3–Te3) = 307.8 pm.[2] The other type of chain can be viewed as a homonuclear polymer of Te1 and Te2 atoms. Within (001) planes Te1 and Te2 atoms form linear Te1–Te2–Te1 units (d(Te1–Te2) = 300.8 pm), which are staggered cross-shaped along [001] to form a branched Te2 chain with the same intrachain distance as the Te3 chain (d(Te2–Te2) = 307.8 pm). These distances are quite unusual in the sense that they are too long for a normal Te–Te single bond (e.g., 271 pm in diphenyl ditelluride (3)) but too short for a nonbonding interaction (> 320 pm). Based on this structural observation, Böttcher and Schewe-Miller (4) have described the arrangement of Te(1) and Te(2) atoms as the stacking of XeF_2-like molecules. This aspect will be examined in our analysis in detail.

The two types of chains are shifted by $\frac{1}{4}\cdot c$ against one another, so that Te1 and Te2 atoms lie at positions $z = 0$ and $z = \frac{1}{2}$, whereas Te3 atoms at $z = \frac{1}{4}$ and $z = \frac{3}{4}$. Tl atoms are situated in the more dense planes of Te1 and Te2 and therefore between the Te3 planes. Te3 atoms are thus coordinated by four Tl atoms above and below in a tetragonal antiprismatic manner (d(Te3–Tl) = 348.9 pm). The shortest distances with Tl atoms are adopted by Te1 atoms, which have within (001) planes four Tl neighbors at d(Te1–Tl) = 340.3 and 343.4 pm, and four further ones at d(Tl–Te1) = 354.3 pm situated in neighboring (001) planes (2 + 2 + 4 coordination). Te2 atoms are the most weakly Tl-coordinated Te species, having only four Tl neighbors at d(Te2–Tl) = 363.9 pm.

The phase transition at 172 K (from space group $I4/mcm$ into space group $P4_2/nmc$) shows characteristics of a Peierls-type distortion, namely the formation of large distance alternations (d(Te2b–Te2b) = 285.5 and 330.2 pm) along [001] for one-half of the branched linear Te2 chains forming discrete $(Te_3)_2$ units. The other half of branched Te2 chains still remains exactly linear equidistant with d(Te2a–Te2a) = 307.9 pm. All the equidistant Te3 chains are only slightly distorted due to a small bending of 5.6° from the exact linear arrangement. For illustration the crystal structure of the LT polymorph is shown in Fig. 1.

The formation of distance alternations along [001] does not lead to a doubling of the unit cell in the [001] direction; instead the crystallographic cell parameters in a_1 and a_2 directions are doubled, giving a tetragonal C-centered cell, which reduces in the conventional setting to a P Bravais type with lattice vectors of $a'_1 = \frac{1}{2}(a_1 + a_2)$ and

[1] To whom correspondence is to be addressed.

[2] In the following all interatomic distances for the RT phase correspond to the $T = 184$ K structure refinement.

0022-4596/01 $35.00

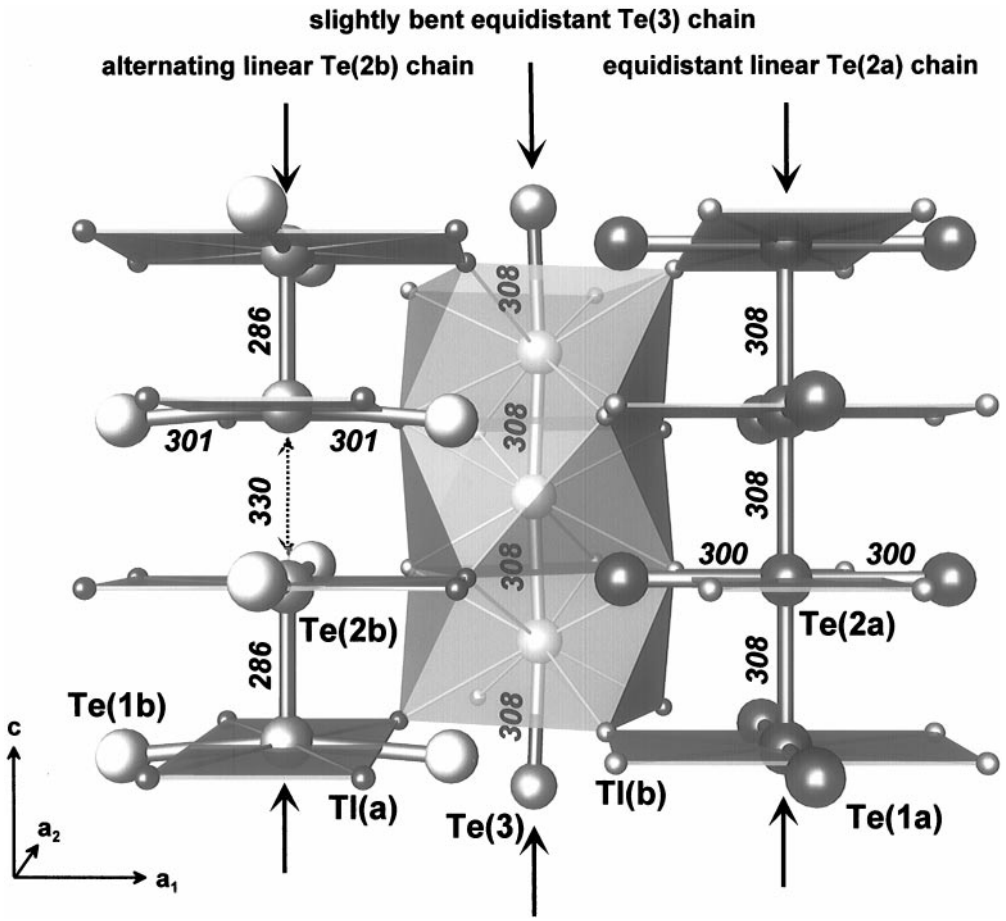

FIG. 1. Crystal structure of LT TlTe. In the RT polymorph all Te chains are exactly linear and equidistant. All distances are in units of pm.

$a'_2 = \frac{1}{2}(a_1 - a_2)$. Former measurements of electrical properties (5) showed that the transition only leads to a slight increase of resistivity by a factor of ≈ 1.2 and not to a semiconducting compound.

DETAILS OF THE ELECTRONIC BAND STRUCTURE CALCULATIONS

LDA LMTO-ASA Calculations

Density functional electronic structure calculations within LDA have been performed with the LMTO-ASA program package of Krier *et al.* (6). The calculations include corrections for the neglect of the interstitial region and the partial waves of higher order ("combined correction"). To reduce the overlap of the atomic spheres, empty interstitial spheres were added to the crystal potential and the basis set. The construction of the ASA radii (given in Table 1) was performed according to an automatical procedure of the program package using the method proposed by Jepsen and Andersen (7). The basis set for the band structure calculations consisted of the Tl(6*s*, 6*p*), the Te (5*s*, 5*p*), and the interstitial 1*s* LMTOs. The Tl(6*d*, 5*f*), Te(5*d*, 4*f*) and interstitial *p* and *d* partial waves were included only in the tails of these LMTOs according to the Löwdin downfolding procedure (7).

The *k*-space integration was performed by the tetrahedron method. Charge self-consistency and properties calculations were obtained from 641 and 231 irreducible *k*-points for the RT and the LT polymorph, respectively.

For a characterization of bonding from the orbital and band energetic point of view we calculated for selected orbital interactions the crystal orbital Hamiltonian population (COHP) (8), which is a Hamiltonian population weighted density of states. As recommended (9), a reduced basis set, in which all empty sphere LMTOs have been downfolded, was used for the COHP calculations.

Brillouin Zone

The primitive translation vectors for the *I*4/*mcm* RT phase were chosen in Cartesian coordinates as $T_1 = (-a/2, a/2, c/2)$, $T_2 = (a/2, -a/2, c/2)$, and $T_3 =$

TABLE 1
Lattice Parameters, Atomic Positions [2], and Muffin Tin Sphere Radii (in pm) Used in the LMTO Calculations

RT polymorph with space group $I4/mcm$ at $T = 184$ K: $a = 1290.04$, $c = 615.64$ pm

Atom	Wyckoff	Symmetry	Position
Tl	16k	*m*..	$x = 0.07940$, $y = 0.22936$ 0
Te1	8h	*m*.2*m*	$x = 0.33515$, $x + 1/2$, 0
Te2	4d	*m.mm*	0, $\frac{1}{2}$, 0
Te3	4a	422	0, 0, $\frac{1}{4}$

Atom	Tl	Te1	Te2	Te3
Sphere radius	198.3	172.3	172.2	176.7
Atom (Wyckoff)	E(16j)	E1(8e)	E2(16l)	E3(32m)
Sphere radius	93.3	79.2	77.5	72.0

LT-polymorph with space group $P4_2/nmc$ at $T = 157$ *K*: $a = 1822.9$, $c = 615.7$ pm

Atom	Wyckoff	Symmetry	Position
Tl(a)	16h	1	$x = 0.07500$, $y = 0.84593$, $z = 0.5077$
Tl(b)	16h	1	$x = 0.15462$, $y = 0.07454$, $z = 0.5055$
Te1a	8g	.*m*.	$\frac{1}{4}$, $y = 0.4145$, $z = 0.0046$
Te1b	8g	.*m*.	$\frac{1}{4}$, $y = 0.9145$, $z = 0.4767$
Te2a	4d	2*mm*.	$\frac{1}{4}$, $\frac{1}{4}$, $z = 0.0032$
Te2b	4c	2*mm*.	$\frac{3}{4}$, $\frac{1}{4}$, $z = 0.0193$
Te3	8f	..2	$x = 0.49673$, x, 1/4

Atom	Tl(a)	Tl(b)	Te1a	Te1b	Te2a
Sphere radius	199.4	198.3	173.9	183.5	173.8
Atom (Wyckoff)	Te2b	Te3	E(8f)	E1(16h)	E2(8f)
Sphere radius	164.7	178.8	106.8	96.0	94.1
Atom (Wyckoff)	E3(8g)	E4(8g)	E5(8g)	E6(8g)	E7(16h)
Sphere radius	83.7	82.3	76.8	74.9	76.7
Atom (Wyckoff)	E8(16h)				
Sphere radius	74.9				

$(a/2, a/2, -c/2)$, where a and c are the conventional lattice parameters. The corresponding primitive translation vectors in reciprocal space are given in Cartesian coordinates as $G_1 = (0, 2\pi/a, 2\pi/c)$, $G_2 = (2\pi/a, 0, 2\pi/c)$, and $G_3 = (2\pi/a, 2\pi/a, 0)$. Because of the shape of the first Brillouin zone (see Fig. 2), there is no high symmetry point Z $(0, 0, \pi/c)$ like in the primitive tetragonal lattice of the low-temperature phase. So, to get information about pure dispersion in the k_z direction, the band structure for the RT phase was calculated additionally along a high-symmetry line starting from outside the first Brillouin zone and showing pure k_z dispersion: From $G = (2\pi/a, 0, 2\pi/c)$ to $Z = (2\pi/a, 0, \pi/c)$, and beyond this point to $M = (2\pi/a, 0, 0)$, back to $G = (0, 0, 0)$, and then to $X = (\pi/a, \pi/a, 0)$ to $P = (\pi/a, \pi/a, \pi/c)$ and finally to $N = (\pi/a, 0, \pi/c)$. High-symmetry points were labeled following Miller and Love (10)

RESULTS AND DISCUSSION

For the discussion of the electronic features orthogonal LMTOs or LMTO linear combinations, which are normalized to unity within the ASA spheres, were projected onto the band structure. The width of such a "fat band" is proportional to the corresponding orbital coefficient, where a maximum width corresponding to 0.7 eV was chosen. Calculations were performed for the structures at $T = 184$ and 157 K, i.e., just above and below the phase transition temperature $T = 172$ K. At these temperatures the cell volumes per formula unit of the two polymorphs are almost equal and simplify direct comparisons. In the following we omit a discussion of the valency of Tl, as it is clear already from crystal chemical considerations (2) that we find Tl^+ in RT and LT TlTe, which is confirmed by our band structure analyses.

Te2 and Te3 Linear Chains

The prominent electronic features are due to the special partial structures of different tellurium ions leading to

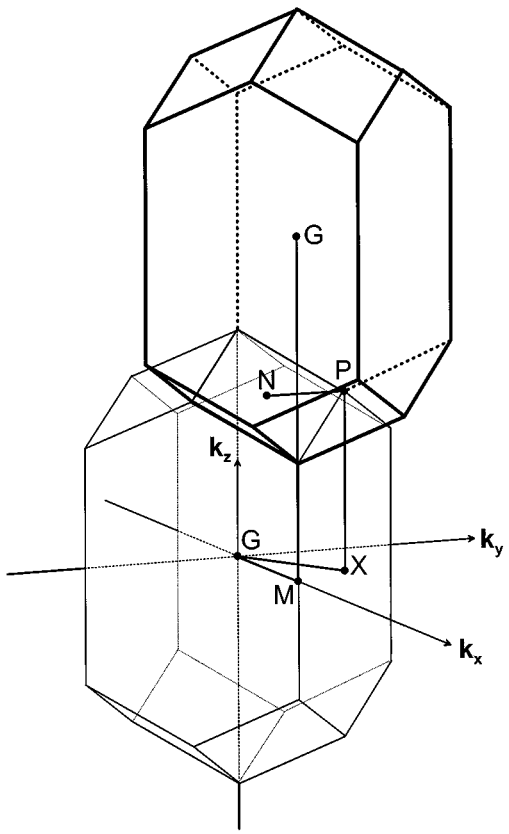

FIG. 2. Brillouin zone of RT TlTe with chosen symmetry lines.

metallic conductivity. Two steep Te majority bands cross the Fermi level. They originate from two separate Te2($5p_z$) and Te3($5p_z$) intrachain band states that have a considerable dispersion along k_z (Figs. 3a and 3b), i.e., $G = (2\pi/a, 0, 2\pi/c)$ to $M = (2\pi/a, 0, 0)$ and X to P. As there are two equidistant Te2 and two equidistant Te3 atoms already in the primitive unit cell, for each type of Te chain the typical backfolded $p_zp_z\sigma$ band dispersion curve along k_z is expected. This is indeed the case along $G = (2\pi/a, 0, 2\pi/c)$ to $M = (2\pi/a, 0, 0)$, an accidental degeneracy occurring half along this line at $Z = (2\pi/a, 0, \pi/c)$. So, the primary cause of the metallic behavior of RT TlTe can be traced back to the existence of linear equidistant Te2 and Te3 chains.

The completely occupied Te3 p_x and p_y bands can be classified as intrachain π and π^* bands. Characteristic for these bands is mixing with Tl s and p states, giving rise to covalent Te3–Tl interactions, which are summarized in Table 2. In contrast to this, Te2 atoms interact less strongly with their Tl neighbors (see COHP(Te2–Tl) in Table 2) as they are four-fold homoatomically coordinated members of a branched one-dimensional polymer of Te1 and Te2 atoms. The suggestion of Böttcher and Schewe-Miller (4) to consider this framework as a staggered arrangement of XeF_2-type Te1–Te2–Te1 molecules turned out to be an interesting starting point for our orbital analysis.

Chains of Linear Triatomic Te1–Te2–Te1 Units

In the following we will extract those bands from the band structure that belong to the Te1/Te2 partial structure and analyze them in terms of the known orbital diagram for linear triatomic 22 valence electron (VE) molecules. To avoid effects of electronegativity difference, we choose symmetric I_3^- as our model molecular system. The general ideas of chemical bonding for this molecule based on MO theory range back to 1951 (11)

The important features for this famous class of molecules are depicted on the left side of Fig. 4: Valence s orbitals can be neglected for this qualitative picture as they interact only very weakly and show no remarkable hybridization with valence p orbitals. There is a complete filling of all six MOs with π symmetry, and also a filling of two out of three MOs of σ symmetry. Therefore the sum over π MOs is nearest-neighbor antibonding, while for the σ MOs it is three-center four-electron bonding. It is known from detailed ab initio studies (12) that central atom d orbital participation in the nonbonding σ and π orbitals occurs only to a minor extent, if the true valence orbitals are well described by the basis set. We note from our LMTO calculations that only small Te $5d$ orbital contributions can be found below E_F. So, in a qualitative discussion of the electronic structure Te $5d$ orbitals can be omitted, although we are aware of their importance in a quantitative understanding of thermodynamic stability.

We now come back to the orbital analysis of the branched linear Te chains. The primitive unit cell already contains two linear Te1–Te2–Te1 units, which are oriented in the [110] and [1$\bar{1}$0] direction, respectively. For the orbital analysis we use a local coordinate system, where we rotate the original crystal axes by 45° counterclockwise around the z axis. Therefore the σ bonds within the Te_3 units are made of p_x orbitals for that unit and of p_y orbitals for the neighboring units in the $\pm z$ direction. For our analysis we choose the Te_3 unit with $p_x\sigma_x$ orbitals. Making normalized linear orbital combinations according to the orbital phases given by the eigenvectors of the triatomic molecule, we can specifically project out the desired fragment orbitals' contributions to the band structure. We do not show all nine p band projections as the bonding and antibonding combinations can much simpler be presented via one Te1–Te2 COHP diagram (Fig. 5a). However Te1–Te2 nonbonding orbital combinations, which are invisible in COHP, are projected onto the band structure (Fig. 5b). The intrafragment σ_x bonding orbital is completely below E_F and shows only weak dispersion (Fig. 5a), as expected. Similar to the 22 VE molecule, the σ_x nonbonding orbital is occupied and lies higher in energy than the σ_x bonding orbital (Fig. 5b), while the σ_x^* band is completely unoccupied (Fig. 5a). In the COHP diagram we can recognize well the energy sequence of orbital interactions: σ_x (occupied), π_y (occupied), π_y^* (occupied), and σ_x^* (unoccupied), where the π_y^* interactions are situated in a region about E_F. While intramolecular π_y-type orbital interactions perpendicular to the Te2 chain direction are completely occupied as in the 22 VE molecule, this does not hold for the π_z orbitals parallel to the chain direction. Due to crystal symmetry, intramolecular π orbital degeneracy can expect to be simply lifted, but another effect is even more important: A schematical diagram is given on the right side of Fig. 4. The p_z orbitals of the central Te2 atoms behave completely different than those in the isolated molecule. They do not mix with Te1 p_z bands to build π_z bonding and antibonding orbitals (compare Figs. 3a and 5d); instead they interact with Te2 atoms of the neighboring Te_3 units in the $\pm z$ direction and form the already mentioned pure Te2 intrachain $p_zp_z\sigma$ and σ^* band with a large dispersion of about 8 eV. Therefore per Te1–Te2–Te1 fragment two completely filled Te1–Te2 nonbonding Te1 p_z orbitals are left back, which interact strongly with neighboring Tl atoms (see below).

Chemical Bonding and Charge Balance

The basic electronic effects now being clarified, in the following we will address the following questions concerning homoatomic chemical bonding and charge balance: What is the difference (i) between 22 VE I_3^- and the Te1–Te2–Te1 units in RT TlTe, (ii) between Te2 and Te3 linear chains, and (iii) between 22 VE I_3^- and linear Te3 chains?

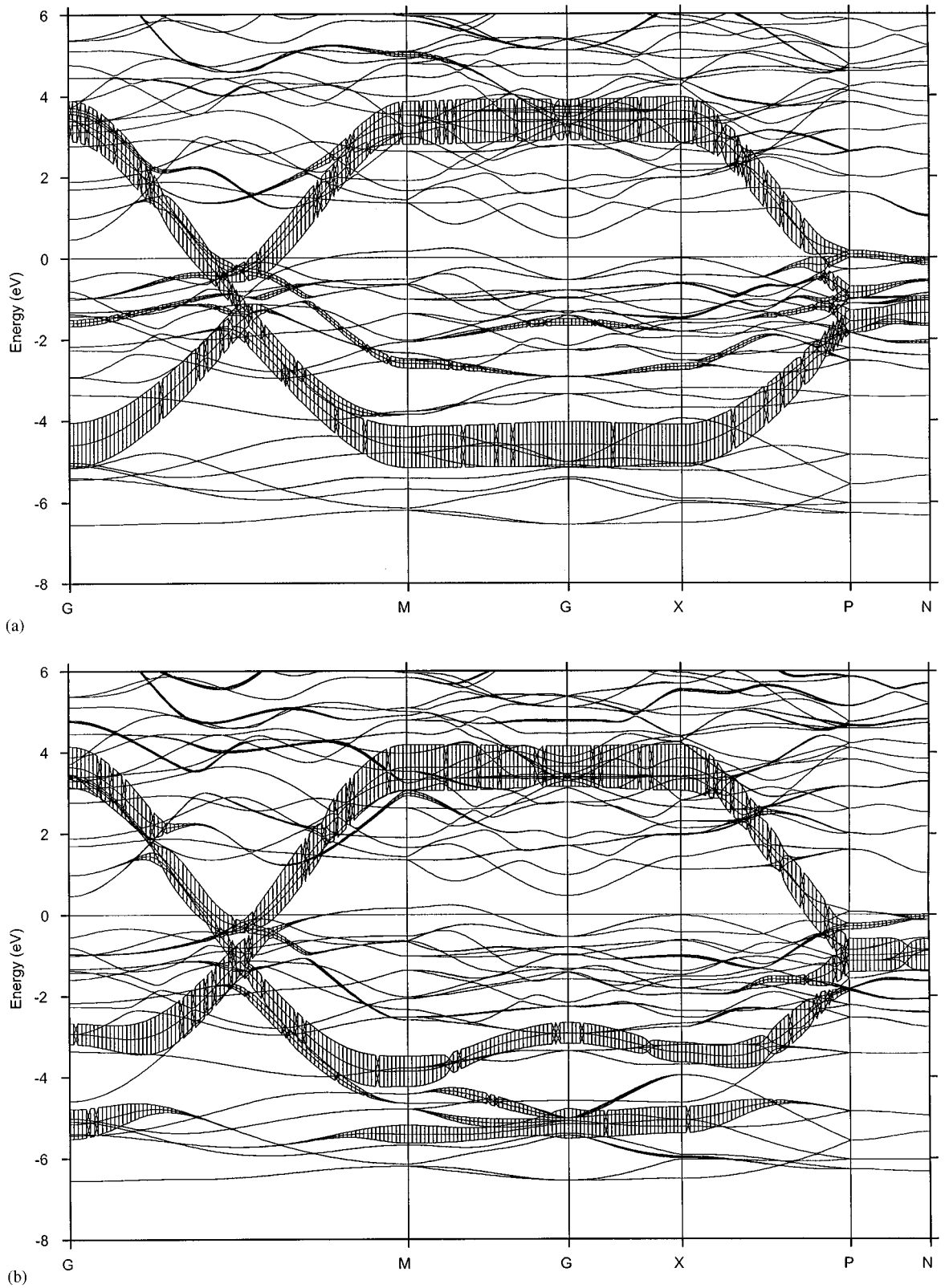

FIG. 3. Energy bands of RT TlTe in the fat band representation: Selected orthonormal orbital characters are projected onto the band structure. A pure state is given the width 0.7 eV. (a) Te2 ($5p_z$) projection, (b) Te3 ($5p_z$) projection.

TABLE 2
Results of the COHP Calculations

T = 184 K		T = 157 K			
Equidistant Te chains		Alternating Te chain		Equidistant Te chain	
Interaction	ICOHP (eV)	Interaction	ICOHP (eV)	Interaction	ICOHP (eV)
Te1–Tl	0.46 (2×), 0.45 (2×), 0.36 (4×)	Te1b–Tl(a,b)	0.52(2×), 0.50 (2×) 0.49 (2×), 0.29 (2×)	Te1a–Tl(a,b)	0.48 (2×), 0.47 (2×) 0.39 (2×), 0.38 (2×)
Te2–Tl	0.19 (4×)	Te2b–Tl(a)	0.18 (4×)	Te2a–Tl(b)	0.21
Te3–Tl	0.34 (8×)			Te3–Tl(a,b)	0.43 (2×), 0.36 (2×) 0.34 (2×), 0.28 (2×)
Tl–Tl	0.24	Tl(a)–Tl(a)	0.24	Tl(b)–Tl(b)	0.25
Te1–Te2	1.13	Te1b–Te2b	1.16	Te1a–Te2a	1.19
Te2–Te2	**0.95($p_z p_z$ 1.19)**	**Te2b–Te2b**	**2.10 ($p_z p_z$ 2.04) 0.23 ($p_z p_z$ 0.48)**	**Te2a–Te2a**	**0.93 ($p_z p_z$ 1.21)**
Te3–Te3	0.82 ($p_z p_z$ **1.08**)			Te3–Te3	0.87 ($p_z p_z$ **1.08**)

Note. ICOHP values are given in electronvolts per cell and bond.

(1) Three-center four-electron σ bonding is similar for Te1–Te2–Te1 in TlTe and linear triatomic 22 VE molecules. The π_y and π_z type of interaction in the 22 VE molecule is antibonding. As the π_z type of interaction is canceled completely for Te1–Te2–Te1, bonding is increased within the fragment, however, without an increase of formal bond order.

(2) As the Te2 $p_z p_z \sigma/\sigma^*$ band is approximately half-occupied, each Te1–Te2–Te1 fragment can be attributed only one electron of it, giving 21 VE $(\text{Te1–Te2–Te1})^{3-}$, i.e., one electron less than in the isolated 22 VE molecule. Concerning a formal charge attribution for Te1 and Te2 atoms in a hypothetical 22 VE Te_3^{4-} molecule, a simple but realistic estimate based on HMO theory (13) gives a difference in

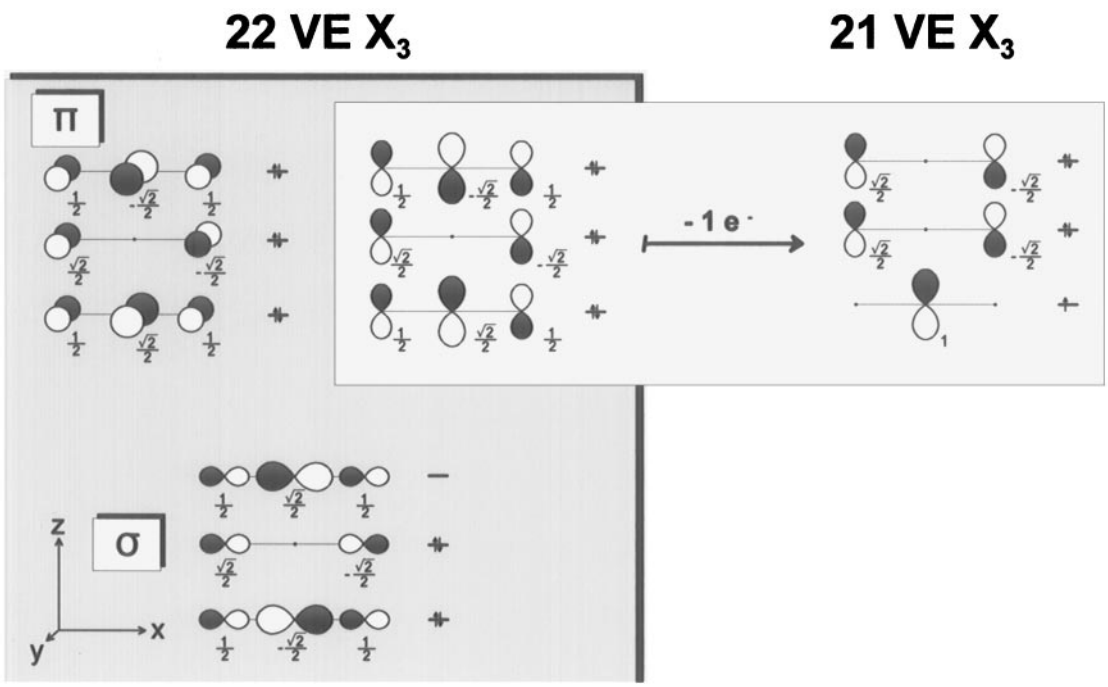

FIG. 4. Scheme for the difference between 22 valence electron homoatomic X_3 molecule (left) and 21 valence electron Te_3 chains in RT TlTe (right) based on HMO theory.

electronic population of 0.5 electrons, with 7.0 electrons on Te2 and 7.5 on Te1 atoms. For our 21 VE molecular fragment, we would expect a charge difference of one additional electron, i.e., in the HMO model 6 electrons on Te2 and 7.5 on Te1. This exactly comes out from a standard extended Hückel calculation (14) calculation (Te (*s*, *p*) basis set, Mulliken population analysis) of the 1D linear equidistant branched chain with 42 electrons per Te_6 unit (band structure: see Fig. 6).

(3) Likewise, we can compare the electronic population of Te3 and Te2. They have the same occupation of p_z orbitals but different intrachain π orbital contributions. Te3 atoms have π_x and π_y orbitals completely (i.e., bonding and antibonding ones) occupied. In contrast, Te2 has only one,

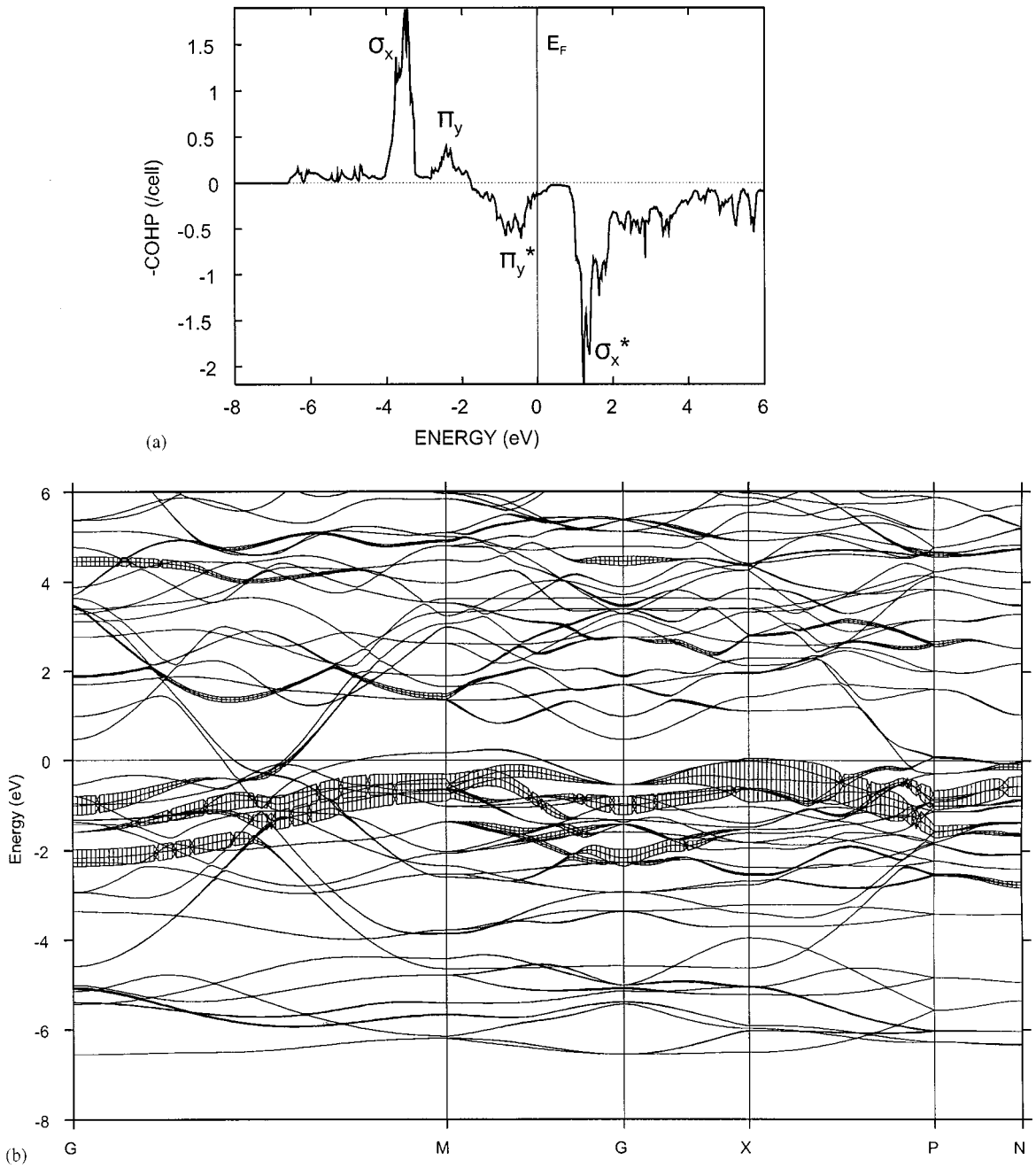

FIG. 5. Characterization of bonding within Te1–Te2–Te1 units for RT phase: (a) COHP, Te1–Te2 ($d = 301$ pm), (b) Te1–Te2–Te1 p_xp_x σ-nonbonding combination, (c) Te1–Te2–Te1 p_yp_y σ-nonbonding combination, and (d) Te1ρ_z orbital projection.

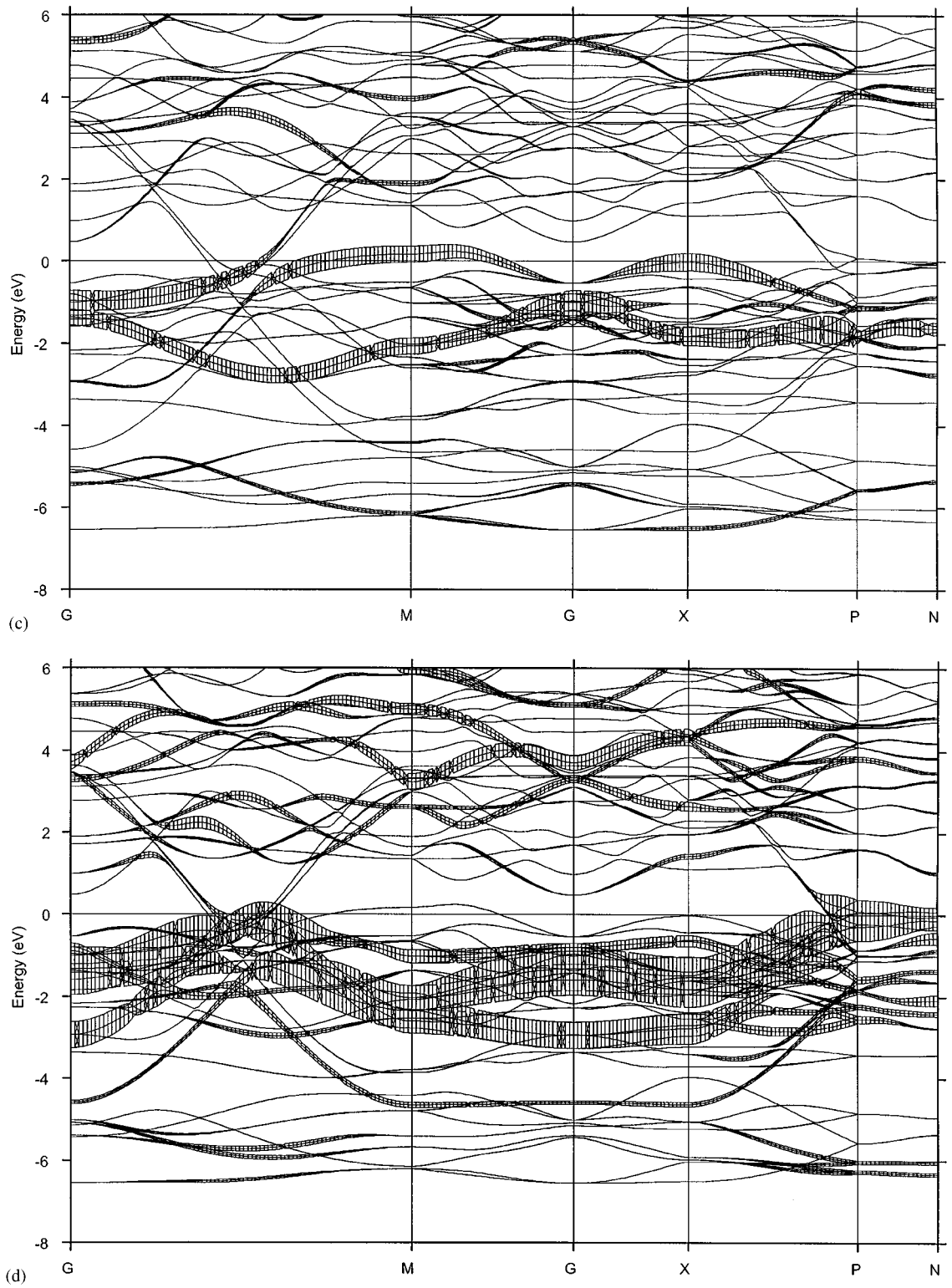

FIG. 5—*Continued*

e.g., π_y, fully occupied (e.g., compare Figs. 7c and 7f). The other one contributes to the Te_3 σ_x-bonding orbital and is therefore only half-occupied (1 electron). On this basis, intrachain bonding should be similar but not identical for Te2 and Te3 chains, Te3 atoms having about one electron more than Te2 atoms, i.e., 7 electrons.

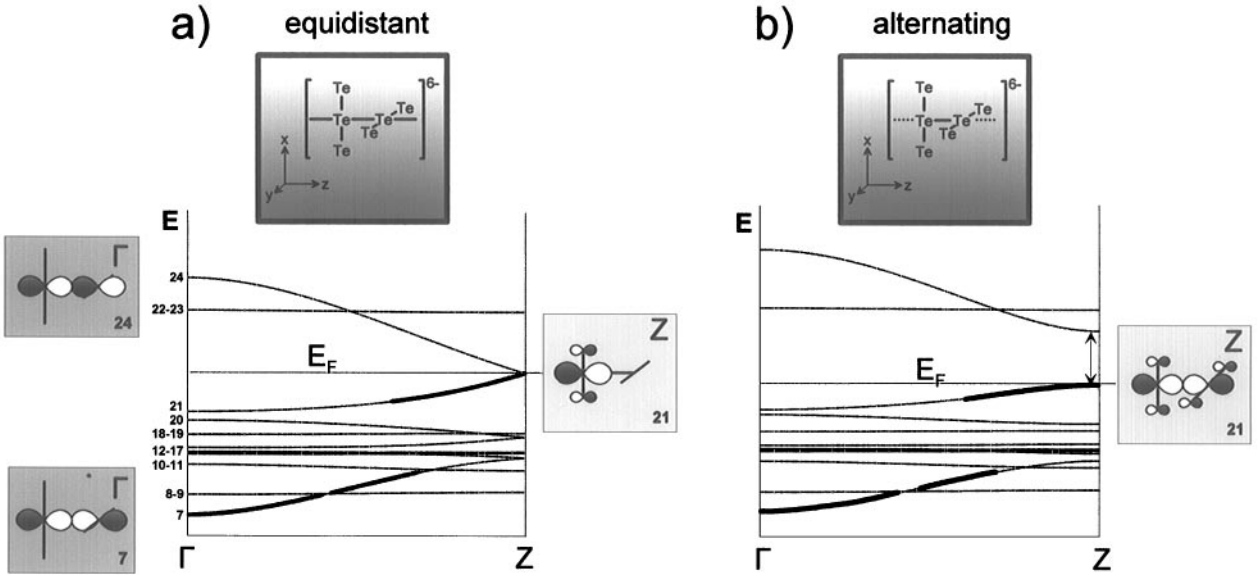

FIG. 6. Schematic representation of the dispersion of an isolated branched linear $(Te1–Te2–Te1)_2$ chain from a 1D-periodic EHT calculation. The six low-lying *s* orbitals are not depicted. Insets show orbital combinations at the zone center and the zone boundary. (a) Equidistant chain (similar to RT TlTe), (b) alternating chain (similar to LT TlTe). The alternating chain exhibits a gap for 42 valence electrons.

Thus, we may summarize the total formal charge balance giving "$(Tl^{+})_8$ $(Te1^{1.5-})_4$ $(Te2^{0})_2$ $(Te3^{1-})_2$."

(4) Comparing the electronic characteristics of the, e.g., I_3^- ion and the (idealized) Te3 chain, we recognize that they are very similar: All π-type bands but only σ bonding and nonbonding bands (situated at *Z*) are occupied, and solely the σ^* states are unoccupied. We can therefore consider the bonding for this type of one-dimensional chains as the solid-state analogue of the 3-center-4-electron bond in linear triatomic 22 VE molecules, which was stated previously by Papoian and Hoffmann (15). The main difference lies in the finite size effect, differentiating the central and terminal atoms in the molecule.

Phase Transition

Having arrived at an estimation for the electronic population of Te3 chain atoms of 7 electrons we note that this partial structure is suspect to a pairing distortion giving $(Te_2)^{2-}$ dumbbells, as was discussed for $ZrTe_3$ previously (16).

Similarly, we may ask whether the one-dimensional $[(Te1–Te2–Te1)_2]^{6-}$ polyanionic partial structure with 42 electrons is also candidate for pairing distortion?

Therefore we show the results of a simple one-dimensional periodic extended Hückel calculation on a branched $[Te_6]$ chain, which can be related well with the LMTO band structure of the full crystal. All in all there are 24 tellurium centered *s* and *p* bands per $[Te_6]$ unit cell. These are depicted in Fig. 6, showing the dispersion relation along the chain direction from *G* to *Z* for an equidistant and for an alternating chain. The latter exhibits the formation of an energy gap at *Z* for a population of 42 electrons, which is exactly the electronic occupation discussed before, i.e., 2×21 electrons. A similar partial gap can be observed for the Te2b p_z bands in the LT polymorph (Figs. 8b and 8c compared to Fig. 8a). So we note that this kind of partial structure is indeed suspect to pairing distortion for an electronic occupation of 42 electrons, which is not surprising in view of our analysis, which came to the result that intrachain σ bonding is similar for Te2 and Te3 chains. Having now identified two possible candidates for pairing distortion, we will deal with the problem of why mainly Te2 and not Te3 chains are distorted during the phase transition at 172 K.

Since the number of formula units of the low-temperature polymorph is twice that of the RT form, the dispersion curves for the LT phase get very hard to follow up, although most details are the same as those in the RT phase. We therefore decided to further analyze the electronic features of the phase transition and the LT phase on the basis of COHP curves for those orbital interactions that play an important role or change essentially.

The projections of the pure intrachain $p_z p_z \sigma$ components (Figs. 7b and 7e, compare to Figs. 7a and 7d) reveal a dominant role for the bonding interactions within both types of chains in the RT phase. These curves look similar to classical one-dimensional Peierls-type systems (as, e.g., the linear equidistant H chain); however there is a decisive difference to this type of systems. A first indication for this can be seen

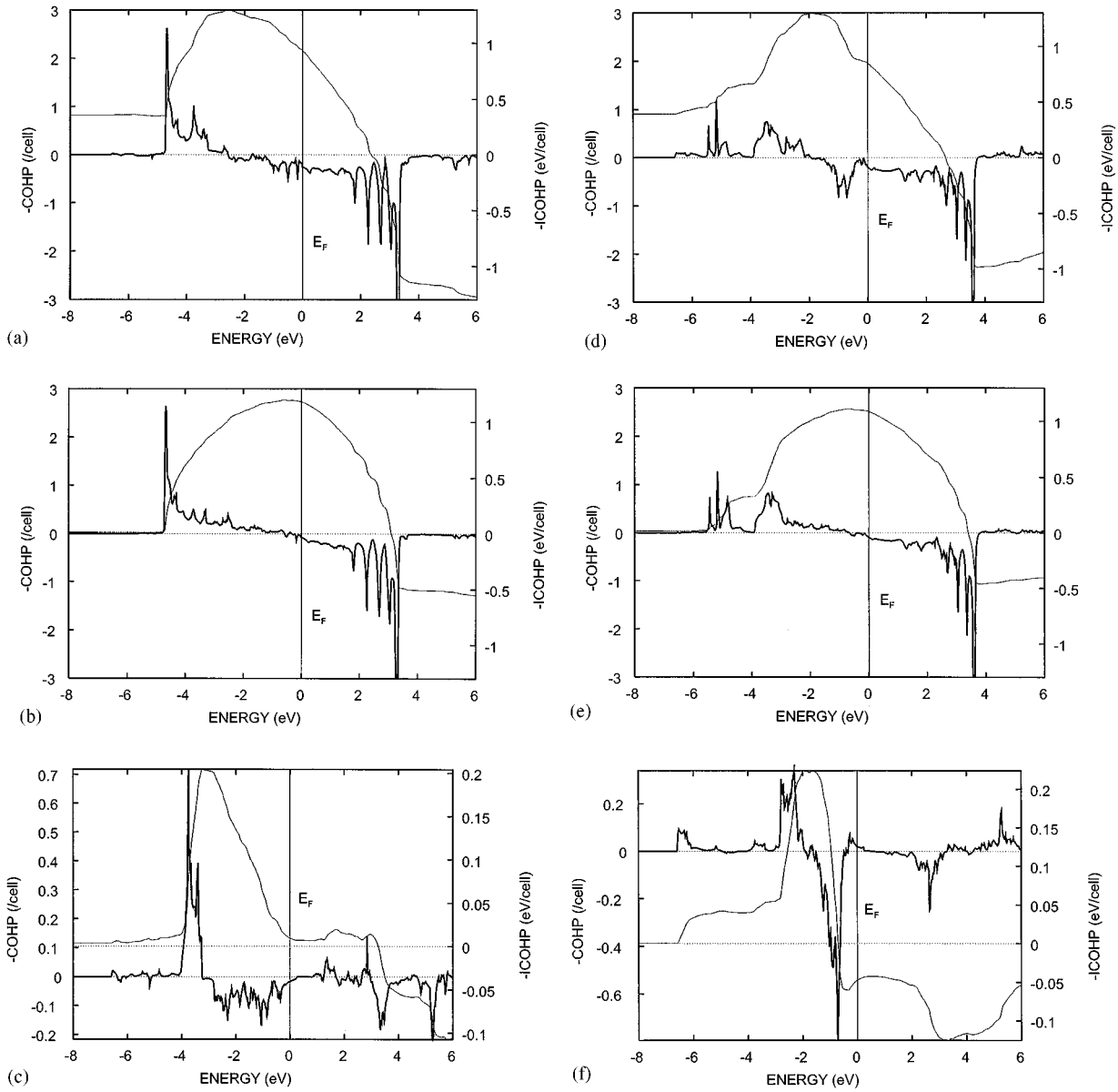

FIG. 7. COHP diagams for RT phase intrachain interactions: (a)–(c) Te2–Te2 interaction: (a) Te2–Te2 ($d = 308$ pm), (b) Te2 (p_z)–Te2(p_z), $p_zp_z\sigma$ contributions, (c) Te2(p_x, p_y)–Te2(p_x, p_y)$p_{x,y}, p_{x,y}\pi$ (d–f) Te3–Te3 interaction, (d) Te3–Te3($d = 308$ pm), (e) Te3(p_z)–Te3(p_z): $p_zp_z\sigma$ contributions, (f) Te3(p_x, p_y)–Te3(p_x, p_y): $p_{x,y}, p_{x,y}\pi$ contributions.

in the Te3–Te3 COHP curve showing a splitting of COHP at lower energies over a certain energy range (Fig. 7e), which is caused by Te3(p_z)–Tl(s) bonding and antibonding interactions along G to M to X. This already shows that the Te3(p_z) bands are significantly influenced by interactions with Tl. We will discuss this point in more detail in the next section (role of Tl).

At $T = 172$ K one-half of the Te2 chains transforms into alternating ones (Te2b chains), the other half remains linear equidistant (Te2a chains). The effect of the distance alternations is clearly signaled by the occurrence of a small non-bonding region above E_F (Fig. 8b) for the $p_zp_z\sigma$ component of COHP(Te2b–Te2b), which is caused by a partial gap in the local density of states. Comparing integrated COHP (ICOHP) for the short and the long Te2b–Te2b distances, we note a much larger value for the former, as expected from bond lengths (for details see Table 2).

It would now be interesting to analyze the local effect on distance alternation by comparing undistorted and distorted chains. From a strict point of view it is not justified to compare COHP and ICOHP values between different systems (8, 17) but we are in the favorable situation that we

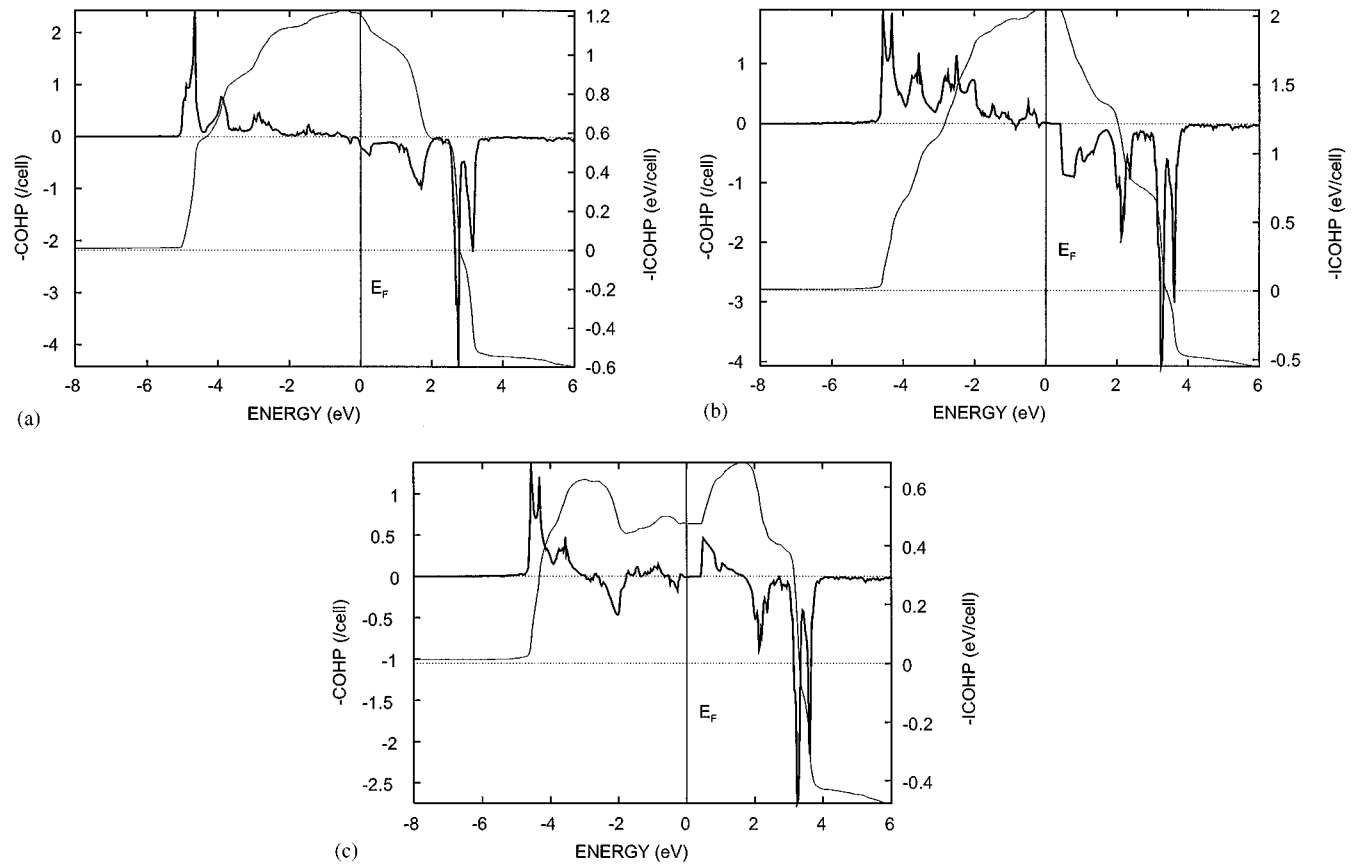

FIG. 8. COHP diagrams for LT phase Te2 p_z intrachain interactions: (a) equidistant chain Te2a–Te2a contact ($d = 308$ pm); (b) alternating chain short Te2b–Te2b contact ($d = 286$ pm); (c) long Te2b–Te2b contact ($d = 330$ pm).

have alternating and equidistant Te chains within the same phase. Using the ICOHP values we can therefore analyze the band energy gain of the Te2b chain on distance alternation compared to equidistant Te2a chains. For this purpose we have slightly adjusted the MT-sphere volumes of the two atom types to exactly the same value, i.e., their average value, since the COHP and ICOHP values depend on the atomic sphere radii. So, sticking closer to the numbers and comparing the undistorted Te2a chain with the distorted Te2b chain, we get ICOHP = 0.93 eV per Te2a–Te2a bond and an average ICOHP = (2.10 + 0.23)/2 = 1.16 eV/bond for each Te2b–Te2b contact. Accordingly, the phase transition leads to an average band energy lowering of 0.23 eV/bond for the Te2b chain. Furthermore, the Te2b–Te2b distance alternation must develop under the constraint that the sum of the short and the long Te2b–Te2b distances is equal to two Te2a–Te2a distances (compare also Fig. 8a with Figs. 8b and 8c). For the $T = 157$ K structure the alternation is even large enough to lead to a situation, where the band energy for the short bond is sufficiently large for a net band energy gain $E_{\text{short}} > 2E_{\text{equi}}$ ($E_{\text{short}} = 2.10$ eV/short bond, $E_{\text{equi}} = 0.93$ eV/bond) so that the small bonding contribution from the longer Te2b–Te2b bond ($E_{\text{long}} = 0.23$ eV) is not important for the qualitative energy balance. This indicates the rather complete character of the distance alternation and may serve to characterize the band energetic properties of the phase transition in a local way.

Role of Tl

Let us now come back to the special role of Tl for the electronic features of this compound and the phase transition.

Both, for the RT and the LT polymorphs, we find Te–Tl orbital interactions whose COHP(E) curves show similar evolvement, starting with bonding contributions at low energies and ending up with some antibonding contributions close to E_F, which is the type of curve expected for orbital interactions between ns^2 cations and closed shell anions and is not shown here. The degree of interactions increases with decreasing interatomic distance, namely ICOHP(Te2–Tl) = 0.19 eV/bond (4 bonds), ICOHP(Te3–Tl) = 0.34 eV/bond (8 bonds), and

ICOHP(Te1–Tl) = 0.46 eV per shortest bond (see Table 2). Taking into account the coordination number of Te2 and Te3 atoms, a large difference on summed orbital interactions with Tl neighbors results ($4 \times 0.19 = 0.76$ eV/Te2 atom, $8 \times 0.34 = 2.72$ eV/Te3 atom), indicating that Te3 is much stronger coordinated by Tl than Te2.

In the energy range of 1 eV below E_F, Tl mixing with Te-centered bands, which are not involved in strong homoatomic σ bonding interactions, is quite strong. This is especially true for the intramolecular π nonbonding orbitals centered on Te1 atoms. Thus, in some parts of the Brillouin zone, due to Te1–Tl antibonding interactions, they lie at higher energies than the π^* bands and even cross E_F in a certain region close to point M (see Fig. 5c). Besides, the intrachain σ bands, they form the second type of bands that cause metallic behavior.

To understand why the system does not simply transform into a semiconductor by introducing completely alternating chains, one must look for differences with classical Peierls-type systems. From the above discussion one point emerges immediately: The bands and the electronic states, which should drive the transition, are not at all separated from bands with other bonding functionality. In fact, they are embedded in a variety of such bands. Therefore, a mechanism like the chain alternation, which lowers the band energy of just this one band near E_F, may increase the energies of others. So, one may ask whether the system is capable at all of being an insulator even with all chains alternating? Test calculations indicate that a semiconducting state is possible in principle but might be difficult to achieve: To open up a gap at Z the chain distortion must be large enough that the antibonding intrachain p_z states, which are already occupied in the RT phase in an energy region of 0.5 to 0.7 eV below E_F (see COHP: p_z–p_z in Figs. 7b and 7e), get shifted above E_F and the top of the intramolecular π nonbonding bands discussed above. A hint that this is possible is demonstrated by one-half of the Te2 atoms, which produce a gap in the local DOS, introducing the observed alternating chain at $T = 172$ K. However to achieve a semiconducting state, quite substantial distance alternations must occur within all the Te2 and Te3 chains, which might be energetically unfavorable (elastic strain) due to structural restrictions imposed by Tl coordination. Closely related to this, is the question, why specifically do Te2 chains distort significantly, and not the Te3 chains? The Te3 chains are embedded in face-sharing tetragonal antiprismatic columns of Tl atoms. An intrachain distance alternation, which leads to a 4 + 4 coordination and a band energy gain for the Te3–Te3 interaction, would simultaneously increase the amount of Te3(p)–Tl(6s) antibonding interactions for Tl atoms with the shorter bond distance, which is a local compensation process and is not expected to be favored above other distortion paths. In contrast to this, Te2 atoms are not coordinated by Tl atoms in such a compact manner; the four Tl neighbors are in the same plane and ICOHP(Te2–Tl) is only half that of ICOHP(Te3–Tl). The Te2–Te1 interaction is not expected to be strongly angle dependent at the onset of a bending distortion, and the slight bending introduced by the phase transition shows no significant changes in the Te1–Te2 interaction (ICOHP(Te1a–Te2a) vs ICOHP(Te1 b–Te2b), see Table 2). Therefore, it is the Te2 chains that exhibit large distance alternations in the LT phase, whereas the Te3 chains show only a very slight bending distortion, which leaves the sum of Te3–Tl interactions practically unaltered (see ICOHP Table 2).

CONCLUSION

Metallic one-dimensional equidistant chains are potentially unstable with respect to pairing distortion (see, e.g., (18)). In favorable cases this is reflected by a corresponding Fermi surface nesting behavior. However, the Fermi surface may not be exclusively determined by one type of bands only. In these cases there may exist either concerted distortion paths, which remove within one step all Fermi surface crossings (i.e., a metal–semiconductor transition occurs), or independent distortion paths that occur only within the single partial structures. The latter situation may not be directly related to a Fermi surface nesting of the full band structure and does therefore not lead to a metal–semiconductor transition in one step. This is the case for TlTe, too.

In the RT phase of TlTe two different Te partial structures, linear equidistant branched and unbranched chains, are simultaneously present. The reason for the metallic behavior of RT TlTe can be attributed to the existence of both types of linear equidistant Te chains. It was shown that the intrachain σ bonding is very similar to that in homoatomic linear triatomic 22 valence electron molecules with "three-center four-electron bonding."

The structural phase transition shows characteristics of a "local Peierls-type distortion," namely a dimerization reaction of two 21 VE molecular units that can be formally regarded as $[Te_3]^{3-}$. COHP analysis clearly shows the band energetic stabilization on distance alternation and supports the idea of an electronically, partial structure driven phase transition that leads only to a gap in the corresponding partial density of states.

In the newly built homoatomic molecular unit $[Te_6]^{6-}$ a normal 2c–2e–σ-bond connects the centers of two perpendicular 21 VE fragments with 3c–4e bonding. It may be related with T-shaped molecules with hypervalent bonding as, e.g., ClF_3. There the central Cl atom is connected via a normal 2c–2e–σ bond to the equatorial F atom and interactions with the axial F ligands are characterized by 3c–4e bonding (19).

An explanation for the preference on distortion of the branched Te1Te2-polymeric chain over the unbranched

chain in terms of interactions of Tl atoms with the chain atoms was given. Due to Te3–Tl interactions Te3 atoms are more tightly coupled to the lattice than Te2 atoms.

All in all the phase transition at $T = 172$ K concerns only part of the polytelluride chains and the compound keeps up its metallic behavior during the phase transition. Only a hump in resistivity is seen from measurements of the electrical properties (5). It will be exciting to work on the next phase transition at still lower temperatures, the study of which is underway.

ACKNOWLEDGMENTS

We gratefully acknowledge the Deutschen Forschungsgemeinschaft and the Fonds der Chemischen Industrie for financial support. F.R.W. thanks R. Kniep, Y. Grin, and M. Kohout for stimulating discussions.

REFERENCES

1. J. Weis, H. Schäfer, B. Eisenmann, and G. Schön, *Z. Naturforsch. B* **29,** 585 (1974).
2. K. Stöwe, *J. Solid State Chem.* **149,** 123 (2000).
3. G. Llabres, O. Dideberg, and L. Dupont, *Acta Crystallogr. Sect. B* **28,** 2438 (1972).
4. P. Böttcher and I. Schewe-Miller, *in* "Unkonventionelle Wechselwirkungen in der Chemie metallischer Elemente" (B. Krebs, Ed.), p. 285. VCH Verlagsgesellschaft, Weinheim, 1992.
5. J. D. Jensen, J. R. Burke, D. W. Ernst, and R. S. Allgaier, *Phys. Rev. B* **6,** 319 (1972).
6. G. Krier, O. Jepsen, A. Burkhardt, and O. K. Andersen, Tight Binding LMTO-ASA Program Version 4.7, Stuttgart, Germany.
7. O. Jepsen and O. K. Andersen, *Z. Phys. B* **97,** 35 (1995).
8. R. Dronskowski and P. E. Blöchl, *J. Phys. Chem.* **97,** 8617 (1993).
9. F. Boucher and R. Rousseau, *Inorg. Chem.* **37,** 2351 (1998).
10. S. C. Miller and W. F. Love, "Tables of Irreducible Representations of Space Groups and Co-Representation of Magnetic Space Groups." Pruett Press, Boulder, CO, 1967.
11. G. C. Pimentel, *J. Chem. Phys.* **19,** 446 (1951); R. J. Hach and R. E. Rundle, *J. Am. Chem. Soc.* **73,** 4321 (1951).
12. H. F. Schaefer III, "The Electronic Structure of Atoms and Molecules: A Survey of Rigorous Quantum Mechanical Results," p. 281. Addison-Wesley, London, 1972.
13. E. E. Havinga and E. H. Wiebenga, *Rec. Trav. Chim. Pays-Bas* **78,** 724 (1959).
14. M.-H. Whangbo, R. Hoffmann, and R. B. Woodward, *Proc. R. Soc. London Ser. A* **366,** 23 (1979).
15. G. A. Papoian and R. Hoffmann, *Angew. Chem. Int. Ed.* **39,** 2408 (2000).
16. K. Stöwe and F. R. Wagner, *J. Solid State Chem.* **138,** 160 (1998).
17. N. Börnsen, B. Meyer, O. Grotheer, and M. Fähnle, *J. Phys.: Condens. Matter* **11,** L287 (1999).
18. E. Canadell and M.-H. Whangbo, *Chem. Rev.* **91,** 965 (1991).
19. W. Kutzelnigg, "Einführung in die Theoretische Chemie," Band 2, p. 375. Verlag Chemie, Weinheim, 1978.